Prototype of a 64-Element Phased Array Transmitter With Wide Axial Ratio Bandwidth and Beamwidth

Mei Qian, Hao Jiang*, Shaowei Liao, Quan Xue
School of Electronic and Information Engineering, South China University of Technology, Guangzhou, China,
qianm@scut.edu.cn; eehaojiang@ieee.org*

***Abstract*—This paper presents the design and implementation of a 64-element phased array transmitter, offering wide axial ratio (AR) bandwidth and beamwidth. The radiating elements feature a symmetric arc-shaped feed structure, providing dual circular polarization to the antenna. Constructing a dual-layer metasurface structure on the top layer enhances the impedance bandwidth, ensuring compliance with communication standards (27.5–31 GHz), while notably expanding the 3-dB AR bandwidth and beamwidth. Sixteen 8-channel beamforming integrated circuits (BFICs) enable independent control of amplitude and phase for the transmitter. Both simulation and experimental results validate the system's performance, demonstrating wide-angle scanning capability, high cross-polarization discrimination (XPD) level, and a wide AR bandwidth (27.5–31 GHz) with a large beamwidth of ±50°.**

***Index Terms*—Phased array transmitter, AR bandwidth, beamwidth, metasurface**

I. Introduction

The rapid growth in demand for global space-based broadband connectivity is being driven by the increasing presence of commercial satellite networks such as Starlink, OneWeb, and Kuiper [1], [2]. These innovative satellite communication (SATCOM) systems are transforming global connectivity by deploying vast constellations of satellites in low Earth orbit (LEO) and medium Earth orbit (MEO), offering high-speed, low-latency coverage across the globe. A critical factor enabling these systems is the advancement of silicon-based beamforming technologies and the development of cost-effective phased array systems. This progress has made it possible to integrate advanced active electronically scanned arrays (AESAs) into user terminals at a significantly lower cost, providing the fast and precise electronic beam steering required to maintain stable communication with satellites in lower orbital planes.

The reduced costs of phased array technology also enhance the performance of geostationary orbit (GEO) SATCOM systems, especially for mobile applications that demand continuous connectivity [3], [4].

In this work, we introduce a wideband, reconfigurable, dual-circular polarization *Ka*-band SATCOM transmit phased array. A shared arc-shaped structure is integrated into the 64-element array, enabling the dual-polarized ports to achieve a high cross-polarization discrimination (XPD). The wide-beam radiation elements provide the array with a wide-angle scanning capability of up to 60°. Unlike previous *Ka*-band phased array designs, the integrated dual-layer metasurface-based dual-circularly polarized radiating element enables broadband and wide-angle impedance matching with free space. This innovation allows the corresponding transmitter to achieve superior and stable axial ratio (AR) performance even under wide-angle beam scanning.

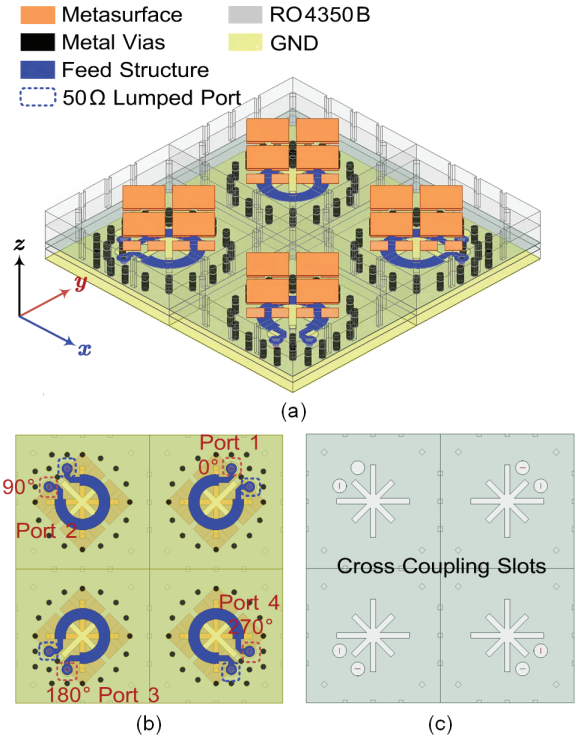

Fig. 1. 2×2 Antenna elements. (a) Front view. (b) Feed structure and rotary phase configuration. (c) Cross-coupling slots.

II. Design and Analysis

A. Antenna Element

Fig. 1(a)-(c) shows a 2×2 antenna elements. The antenna employs a multilayer RO4350B substrate with a low-loss dielectric. The bottom layer serves as a ground (GND) plane, providing RF grounding and shielding. The feed port is located at the base of the blue metallic post, where a microstrip-to-coaxial transition (not shown) can be utilized for feeding [see Fig. 1(b)]. Metallic vias (black parts) within the substrate construct an EM shielding cavity. Above this, the blue arc-shaped feed structure is physically connected to each antenna

978-88-31299-10-7/25/$31.00 ©2025 IEEE

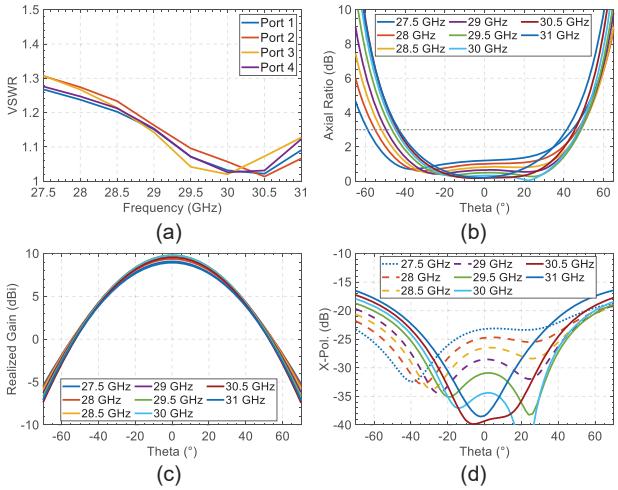

Fig. 2. Simulated performance of the 2×2 antenna elements. (a) VSWR. (b) AR. (c) Realized gain. (d) Cross polarization amplitude.

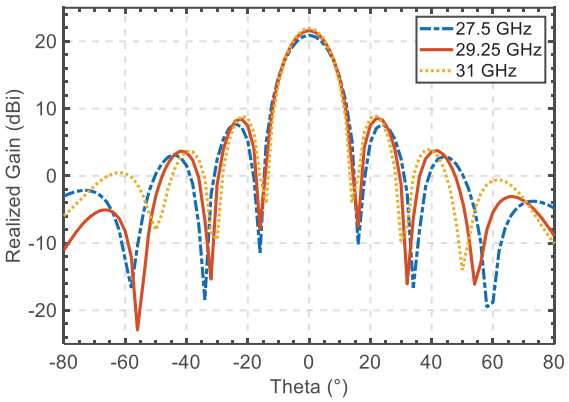

Fig. 3. Simulated on-axis realized gain of the 64-element phased-array antenna under LHCP.

element, controlling two ports for left-hand circular polarization (LHCP) and right-hand circular polarization (RHCP), respectively. As EM waves in the feed structure pass through each cross-shaped slot [see Fig. 1(c)], sequentially coupled linearly polarized waves synthesize the corresponding circularly polarized waves. The topmost layer comprises a dual-layer metasurface structure (orange parts), which serves as the antenna's radiating elements, converting RF energy into EM waves in free space. Compared with traditional microstrip patches, the use of double-layer metasurfaces significantly broadens the impedance bandwidth.

The radiation boundary conditions are implemented for full-wave simulations using HFSS software. Since each antenna element is inherently circularly polarized, we apply sequential rotational phase configurations to the rotationally symmetric antenna elements in the model, assigning phase shifts of 0°, 90°, 180°, and 270° for the four ports, respectively [see Fig. 1(b)].

Fig. 2(a)–(d) show the simulated performance as follow:

1) The voltage standing wave ratio (VSWR) of the four ports is still below 1.3 within 27.5–31 GHz, enabling good impedance matching.
2) The 3-dB AR beam-width exceeds ±40° across the frequency sweep from 27.5 to 31 GHz, and the on-axis (θ = 0°) AR consistently remains below 3 dB, indicating a relatively wide AR bandwidth.
3) The realized gains of the four elements exceed 8.5 dBi at all frequencies, and the 3-dB beamwidths are all over 80°.
4) At all frequencies, the on-axis (θ = 0°) XPD exceeds 23 dB, and within a scanning range of ±60°, the XPD remains greater than 16 dB.

B. Antenna Array

We further established radiation boundary conditions and extended each of the four antenna elements shown along both the x- and y-axis four times, expanding the array to 64 elements. Taking LHCP waves as an example, the simulated on-axis realized gain of the 64-element phased-array antenna exceeds 20.5 dBi, and the sidelobe level (SLL) exceeds 12 dB for the frequencies of 27.5, 29.25, and 31 GHz, as shown in Fig. 3.

Fig. 4 presents the simulated beam patterns at three frequencies for LHCP waves. The array exhibits wide-angle scanning capabilities, with gain drops of 3-dB, 4-dB, and 6.5-dB at 60° scanning angles for 27.5, 29.25, and 31 GHz, respectively. The SLL versus scan angle exceeds 10 dB at all frequencies.

C. Transmitter System

As shown in Fig. 5, the configuration comprises a metasurface antenna constructed by stacking multiple layers of printed circuit boards (PCBs) from bottom to top. These multilayer PCBs provide essential structural support and electrical interconnections. Embedded within the substrate are RHCP and LHCP feed networks dedicated to radio frequency (RF) signal control. At the uppermost level, interfaces of beamforming chips connect to power supplies, control units, and RF connection components, ensuring signal transmission and control functionalities. The topmost layer features a ball grid array (BGA) formed by beamforming chips capable of dynamically adjusting amplitude and phase.

III. Measurement and Discussion

A. Manufacturing Prototype

Fig. 6 presents the manufactured prototype of the transmitter. This prototype employs 16 transmit beamforming integrated circuits (BFICs) to control the antenna array. Each BFIC drives four antenna unit cells, resulting in a total of 64 antenna elements. The RF signal is distributed to each transmit chip through a 1-to-16 Wilkinson power divider, achieving uniform signal distribution and low-loss transmission. Fig. 6(a) illustrates the front side of the circuit board, where the digital control section is on the left, while Fig. 6(b) shows the 64-element antenna array composed of radiation modules.

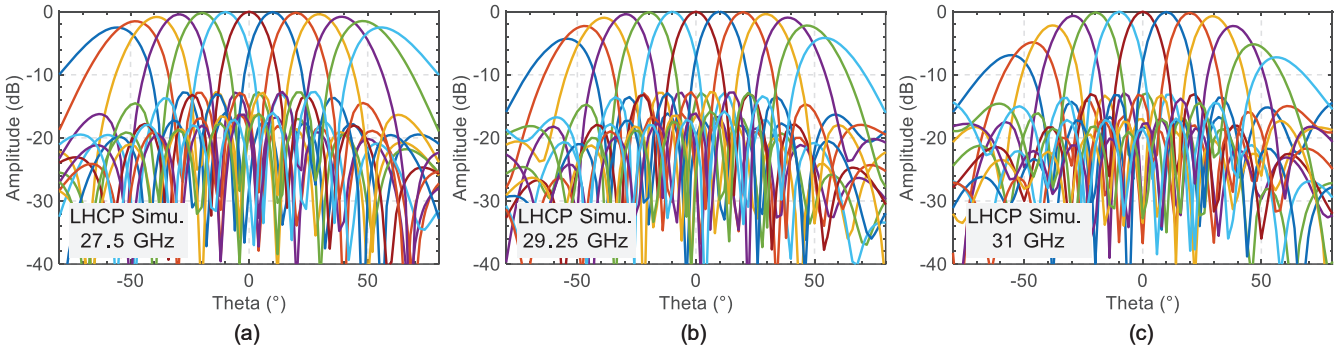

Fig. 4. Simulated scanned beams at (a) 27.5, (b) 29.25, and (c) 31 GHz for LHCP waves (ϕ = 0°).

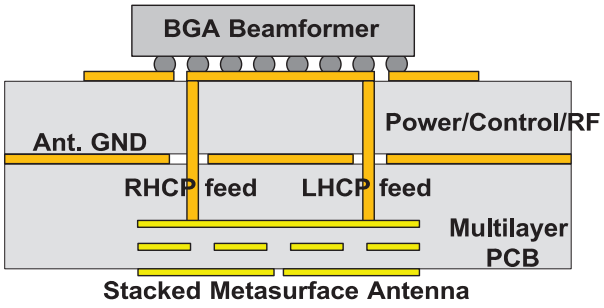

Fig. 5. Configuration from antenna end to beamforming chip.

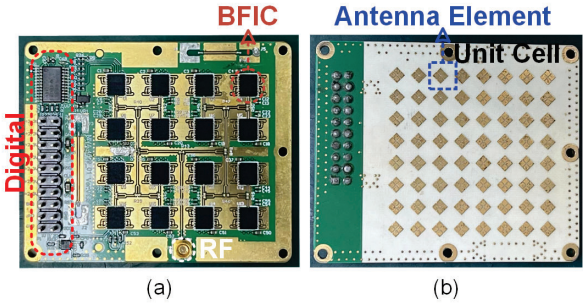

Fig. 6. Manufacturing prototype. (a) Back view. (b) Front view

B. Measurement

The proposed prototype underwent experimental measurement, and various performance metrics, such as on-axis beam characteristics, XPD, AR bandwidth, and AR beamwidth, are evaluated.

1) The measured on-axis 3-dB beamwidth is approximately 12.5°, and the measured XPDs all exceed 19 dB.
2) The measured 3-dB AR bandwidth on axis (θ = 0°) agrees well with simulated ones, and it consistently covers 27.5–31 GHz.
3) As shown in Fig. 9(a)-(c), the simulated 3-dB AR beamwidth exceeds ±50° across the frequency sweep from 27.5 to 31 GHz.

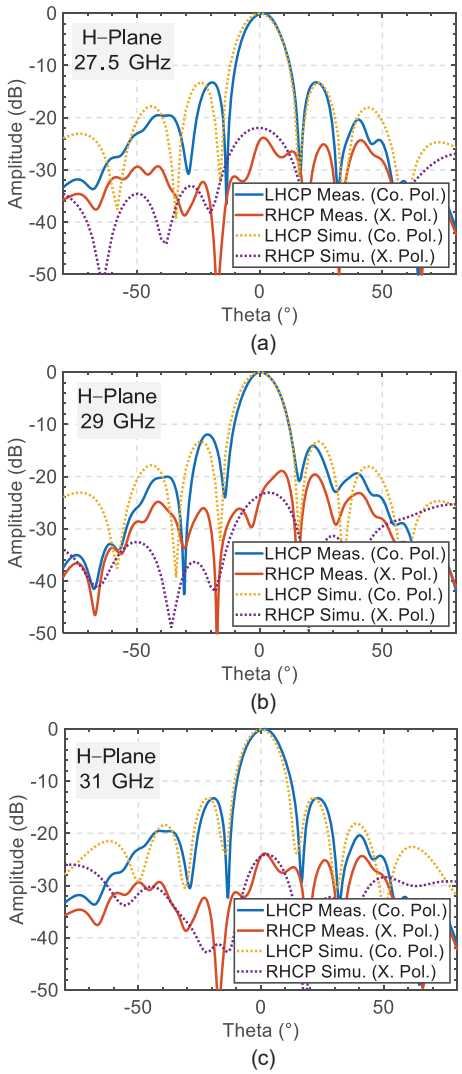

Fig. 7. Measured and simulated co-polarization and cross-polarization amplitudes for LHCP at (a) 27.5, (b) 29, and (c) 31 GHz (H-plane) on axis.

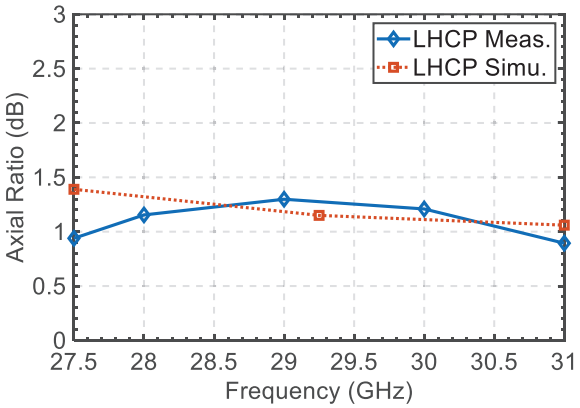

Fig. 8. Measured and simulated AR versus the frequency.

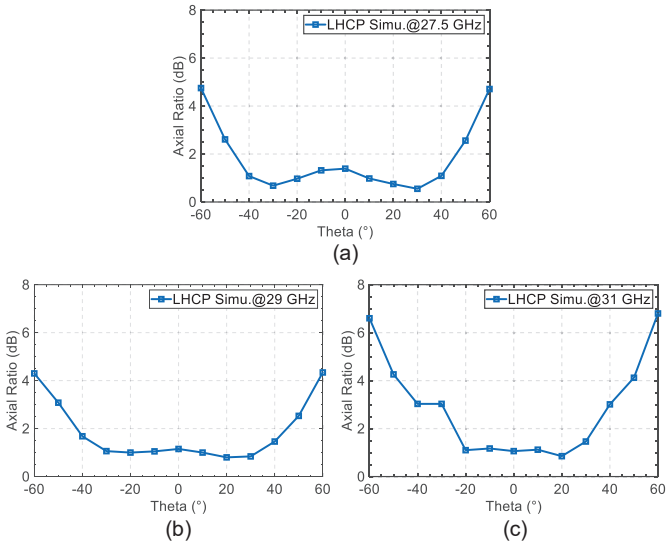

Fig. 9. Simulated AR versus the scanned angle at (a) 27.5, (b) 29, and (c) 31 GHz (H-plane).

C. Comparison and Discussion

Compared with other designs, the main features and contributions of this work can be summarized as follows:

1) High-integration design and low-cost implementation: The RF circuitry and digital control sections are highly integrated using PCB technology, particularly through the incorporation of BFICs. This integration results in a compact system size, reduced complexity, and enhanced system performance.
2) Dual-port dual circular polarization capability for each antenna element: Each antenna element supports dual-port dual circular polarization without the need for rotational phase configuration of multiple linearly polarized elements. This configuration effectively reduces the number of active channels and lowers power consumption.
3) Phased array antenna integrating dual-layer metasurfaces: The transmitter system integrates dual-layer metasurfaces, which effectively extend the operating bandwidth to cover satellite uplink communication standards.
4) Wide AR bandwidth and beamwidth: The transmitter features a broad 3-dB AR bandwidth covering 27.5–31 GHz and an AR beam-width exceeding 50°.
5) Advanced beamforming technology: By digitally controlling the active BFICs and integrating RF-integrated circuit control, the system provides flexible and dynamic beamforming capabilities.

IV. Conclusion

This work presents a 64-element phased array transmitter with dual circular polarization properties. BFICs provide independent amplitude and phase control. Simulations and measurements confirm its wide-angle scanning (±60°), high XPD, and wide AR bandwidth (27.5–31 GHz) with an AR beamwidth of ±50°.

V. Acknowledgments

This work was supported by the Guangdong Innovative and Entrepreneurial Research Team Program under Grant 2017ZT07X032, the National Natural Science Foundation of China under Grant 62271212, Guangdong Basic Applied Basic Research Foundation Grant Outstanding Youth Fund Project under Grant 2021B1515020039, and Fundamental Research Funds for the Central Universities under Grant 2023ZYGXZR004.

References

[1] I. del Portillo, B. G. Cameron, and E. F. Crawley, "A technical comparison of three low earth orbit satellite constellation systems to provide global broadband," *Acta Astronautica*, vol. 159, pp. 123–135, Jun. 2019.
[2] S. Burleigh, T. Cola, S. Morosi, S. Jayousi, E. Cianca, and C. Fuchs, "From connectivity to advanced internet services: A comprehensive review of small satellites communications and networks," *Wireless Commun. Mobile Comput.*, vol. 2019, pp. 1–17, May 2019.
[3] L. Paulsen et al., "Fabrication and measurement of a large, monolithic, PCB-based AESA," in *Proc. IEEE Int. Symp. Phased Array Syst. Technol. (PAST)*, Oct. 2016, pp. 1–7.
[4] T. Takahashi et al., "Wide-angle beam steering AESA with threedimensional stacked PCB for *Ka*-band in-flight connectivity," in *Proc. IEEE Int. Symp. Phased Array Syst. Technol. (PAST)*, Oct. 2019, pp. 1–5.
[5] K. K. W. Low, G. M. Rebeiz, S. Zihir, and T. Kanar, "A reconfigurable dual-polarized 1024-element *Ka*-band SATCOM transmit phased-array with large scan volume and +48 dBW EIRP," in *IEEE MTT-S Int. Microw. Symp. Dig.*, Jun. 2021, pp. 638–640.
[6] K. K. W. Low, A. Nafe, S. Zihir, T. Kanar, and G. M. Rebeiz, "A scalable circularly-polarized 256-element *Ka*-band phased-array SATCOM transmitter with ±60° beam scanning and 34.5 dBW EIRP," in *IEEE MTT-S Int. Microw. Symp. Dig.*, Jun. 2019, pp. 1064–1067.
[7] K. K. W. Low, S. Zihir, T. Kanar, and G. M. Rebeiz, "A scalable switchable dual-polarized 256-element *Ka*-band SATCOM transmit phased array with embedded RF driver and ±70 beam scanning," in *IEEE MTT-S Int. Microw. Symp. Dig.*, Aug. 2020, pp. 821–824.
[8] A. Nafe, M. Sayginer, K. Kibaroglu, and G. M. Rebeiz, "2×64 dual polarized dual-beam single-aperture 28 GHz phased array with high cross-polarization rejection for 5G polarization MIMO," in *IEEE MTT-S Int. Microw. Symp. Dig.*, Jun. 2019, pp. 484–487.
[9] A. Nafe, M. Sayginer, K. Kibaroglu, and G. M. Rebeiz "2×64-element dual-polarized dual-beam single-aperture 28-GHz phased array with 2×30 Gb/s links for 5G polarization MIMO," *IEEE Trans. Microw. Theory Techn.*, vol. 68, no. 9, pp. 3872–3884, Jun. 2020.
[10] W. M. Abdel-Wahab et al., "A modular architecture for wide scan angle phased array antenna for K/Ka mobile SATCOM," in *IEEE MTT-S Int. Microw. Symp. Dig.*, Jun. 2019, pp. 1076–1079.